16th Australasian Fluid Mechanics Conference
Crown Plaza, Gold Coast, Australia
2-7 December 2007

Skin friction Reduction by Introduction of Micro-bubbles into Turbulent Boundary Layer

K. Mohanarangam[1], C.P. Cheung[1], J. Y. Tu[1] & L.Chen[2]

[1]School of Aerospace, Mechanical and Manufacturing Engineering
RMIT University, Vic. 3083, Australia
[2]Maritime Platforms division,
DSTO, Maribyrnong, Vic. 3032, Australia

ABSTRACT

The phenomenon of drag reduction by the injection of micro-bubbles into turbulent boundary layer has been investigated using an Eulerian-Eulerian two-fluid model. Two variants namely the Inhomogeneous and MUSIG (MUltiple SIze Group) based on Population balance models are investigated. The simulated results are compared against the experimental findings of Madavan et al [1]. The model employed in the investigation comprises of a two-dimensional micro-bubble laden flow wherein the Reynolds averaged Navier-Stokes (RANS) transport equations were used to describe both the phases of the flow. A SST (Shear Stress Transport) turbulence model is used as the turbulent closure for the primary phase and a zero equation turbulence model is used for the micro-bubbles.

INTRODUCTION

Numerous experimental and numerical studies have been carried out to investigate the aura of micro-bubbles along the turbulent boundary layer. The mere subsistence of the micro-bubbles seems to reduce the skin friction along the boundary layer for single phase flows. The pursuits of drag reduction by the shear presence of micro-bubbles have wide range of applications for ships, ship tankers of more prominence and to increase the efficiency of fluids which succumbs to long distance transport through pipelines. Micro-bubbles have a greater role of reducing drag for submarines, wherein the wetted surface of the vessel is 100%. Two broad theories can be spelled out from the micro-bubble drag reduction. Firstly, the drag reduction is attributed towards the material properties of the carrier (water) and the dispersed phase (mostly air), called the density ratio effect, wherein the density ratio between the phases is fairly high, as a result causing an elevated mixture viscosity and a reduced turbulent momentum transfer due to the dispersed phase, there by causing a subsequent drop in wall shear stress and hence the skin-friction [2]. The second theory proposes that micro-bubble drag reduction is caused by turbulence distortion along the single phase boundary layer and the relative change instilled by it onto to the dispersed phase have received a heightened importance in recent years both numerically and experimentally[3,4,5,6]

In this paper, the role of the micro-bubble in drag reduction has been numerically investigated. For this endeavor, two different numerical models namely the Inhomogeneous two-fluid and the population balance models have been employed. Population balance models have been employed to take in account of the break-up and the coalescence prevalent at higher gas injection rates. The skin friction co-efficient ratios are compared against the experimental results of Madavan et al [1]. Streamwise velocity modulation effected due to the presence of micro-bubbles have been investigated along the boundary layer, this helps to shed more light on the change effected along the various regions of the turbulent boundary layer in the presence of the micro bubbles. This has been done by validating our numerical model results against most of the well established results; this is carried out in methodical manner in such an order to ensure the validity of our study.

GOVERNING EQUATIONS

Inhomogeneous Two-Fluid model

Mass conservation

Numerical simulations presented in this paper are based on the two-fluid model Eulerian-Eulerian approach. The liquid phase is treated as the carrier phase while the gas phase (bubbles) is considered as dispersed phase (ANSYS, 2006). In isothermal flow condition, with no interfacial mass transfer, the continuity equation of the two-phases with reference to Ishii [7] and Drew and Lahey [8] can be written as:

$$\frac{\partial(\rho_i \alpha_i)}{\partial t} + \nabla \cdot (\rho_i \alpha_i \vec{u}_i) = 0 \qquad (1)$$

where α, ρ and $\vec{u}$ is the void fraction, density and velocity of each phase. The subscripts $i = l$ or g denotes the liquid or gas phase.

Momentum conservation

The momentum equation for the two-phase can be expressed as follow:

$$\frac{\partial(\rho_i \alpha_i \vec{u}_i)}{\partial t} + \nabla \cdot (\rho_i \alpha_i \vec{u}_i \vec{u}_i) = -\alpha_i \nabla P + \alpha_i \rho_i \vec{g} + \nabla \cdot \left[\alpha_i \mu_i^e \left(\nabla \vec{u}_i + (\nabla \vec{u}_i)^T\right)\right] + F_i \qquad (2)$$

On the right hand side of Eq. (2), F_i represents the total interfacial force calculated with averaged variables, $\vec{g}$ is the gravity acceleration vector and P is the pressure. The term F_{lg} represents the inter-phase momentum transfer between gas and liquid due to the drag force resulted from shear and drag which is modelled according to Ishii and Zuber [9] as:

$$F_{\mathrm{lg}}^{\mathrm{drag}} = -F_{\mathrm{gl}}^{\mathrm{drag}} = \frac{1}{8} C_D a_{if} \rho_l \left|\vec{u}_g - \vec{u}_l\right| \left(\vec{u}_g - \vec{u}_l\right) \qquad (3)$$

where C_D is the drag coefficient which can be evaluated by correlation of several distinct Reynolds number regions for individual bubbles proposed by Ishii and Zuber [9].

Interfacial Area Density

In Eq.(3), interfacial momentum transfer due to the drag force is directly dependent on the contact surface area between the two phases and is characterized by the interfacial area per unit volume between gas and liquid phase, named as the interfacial area density a_{if}. Based on the particle model, assuming that liquid phase is continuous and the gas phase is dispersed, the interfacial area per unit volume is then calculated based on the Sauter mean bubble diameter d_g given by

$a_{if} = \frac{6\alpha_g^*}{d_g}$ where

$$\alpha_g^* = \begin{cases} \max(\alpha_g, \alpha_{\min}) if\ (\alpha_g < \alpha_{\max}) \\ \max(\frac{1-\alpha_g}{1-\alpha_{\max}}\alpha_{\max}, \alpha_{\min}) if\ (\alpha_g > \alpha_{\max}) \end{cases}$$

The non-dimensional inter-phase transfer coefficients can be correlated in terms of the particle Reynolds number and is given by

$$\mathrm{Re}_{lg} = \frac{\rho_l |U_g - U_l| d_g}{\mu_l}$$

where μ_l is the viscosity of the liquid phase.

MUSIG Model

To account for non-uniform bubble size distribution, the MUSIG model employs multiple discrete bubble size groups to represent the population balance of bubbles. Assuming each bubble class travel at the same mean algebraic velocity, individual number density of bubble class *i* based on Kumar and Ramkrishna [10] can be expressed as:

$$\frac{\partial n_i}{\partial t} + \nabla \cdot (\vec{u}_g n_i) = \left(\sum_j R_j \right)_i \qquad (4)$$

where $\left(\sum_j \boldsymbol{R}_j\right)_i$ represents the net change in the number density distribution due to coalescence and break-up processes. The discrete bubble class between bubble volumes v_i and v_{i+1} is represented by the centre point of a fixed non-uniform volume distributed grid interval. Tthe interaction term $\left(\sum_j R_j\right)_i = (P_C + P_B - D_C - D_B)$ contains the source rate of P_C, P_B, D_C and D_B, which are, respectively, the production rates due to coalescence and break-up and the death rate due to coalescence and break-up of bubbles.

MUSIG Break-up rate

The production and death rate of bubbles due to the turbulent induced breakage is formulated as:

$$P_B = \sum_{j=i+1}^{N} \Omega(v_j : v_i) n_j$$

$$D_B = \Omega_i n_i \qquad \text{with} \quad \Omega_i = \sum_{k=1}^{N} \Omega_{ki} \qquad (5)$$

Here, the break-up rate of bubbles of volume v_j into volume v_i is modelled according to the model developed by Luo and Svendsen [11]. Similar to the aforementioned ABND models, the model is developed based on the assumption of bubble binary break-up under isotropic turbulence situation. The major different is the daughter size distribution have been taken account using a stochastic breakage volume fraction f_{BV}. By incorporating the increase coefficient of surface area, $c_f = [\, f_{BV}^{2/3} + (1-f_{BV})^{2/3} - 1]$, into the breakage efficient, the break-up rate of bubbles can be obtained as:

$$\frac{\Omega(v_j : v_i)}{(1-\alpha_g) n_j} = F_B C \left(\frac{\varepsilon}{d_j^2} \right)^{1/3} \int_{\xi_{\min}}^{1} \frac{(1+\xi)^2}{\xi^{11/3}} \times \exp\left(-\frac{12 c_f \sigma}{\beta \rho_l \varepsilon^{2/3} d^{5/3} \xi^{11/3}} \right) d\xi \qquad (6)$$

where $\xi = \lambda / d_j$ is the size ratio between an eddy and a particle in the inertial sub-range and consequently $\xi_{min} = \lambda_{min} / d_j$ and *C* and β are determined, respectively, from fundamental consideration of drops or bubbles breakage in turbulent dispersion systems to be 0.923 and 2.0.

MUSIG Coalescence rate

The number density of individual bubble groups governed by coalescence can be expressed as:

$$P_C = \frac{1}{2} \sum_{k=1}^{i} \sum_{l=1}^{i} \eta_{jki} \chi_{ij} n_i n_j$$

$$\eta_{jki} = \begin{cases} (v_j + v_k) - v_{i-1} / (v_i - v_{i-1}) & \text{if } v_{i-1} < v_j + v_k < v_i \\ v_{i+1} - (v_j + v_k) / (v_{i+1} - v_i) & \text{if } v_i < v_j + v_k < v_{i+1} \\ 0 & \text{otherwise} \end{cases}$$

$$D_C = \sum_{j=1}^{N} \chi_{ij} n_i n_j \qquad (7)$$

As discussed in the previous section, bubble coalescence occurs via collision of two bubbles which may be caused by wake entrainment, random turbulence and buoyancy. However, only turbulence random collision is considered in the present study as all bubbles are assumed to be spherical (wake entrainment becomes negligible). Furthermore, as all bubbles travel at the same velocity in the MUSIG model, buoyancy effect is also eliminated. The coalescence rate considering turbulent collision taken from Prince and Blanch [12] can be expressed as:

$$\chi_{ij} = F_C \frac{\pi}{4} \left[d_i + d_j \right]^2 \left(u_{ti}^2 + u_{tj}^2 \right)^{0.5} \exp\left(-\frac{t_{ij}}{\tau_{ij}} \right) \qquad (8)$$

where τ_{ij} is the contact time for two bubbles given by $(d_{ij}/2)^{2/3} / \varepsilon^{1/3}$ and t_{ij} is the time required for two bubbles to coalesce having diameter d_i and d_j estimated to be $[(d_{ij}/2)^3 \rho_l / 16\sigma]^{0.5} \ln(h_0 / h_f)$. The equivalent diameter d_{ij} is calculated as suggested by Chesters and Hoffman [13]: $(d_{ij} = (2/d_i + 2/d_j)^{-1}$. According to Prince and Blanch [12], for air-water systems, experiments have determined the initial film thickness h_o and critical film thickness h_f at which rupture occurs as 1×10^{-4} and 1×10^{-8} m respectively. The turbulent velocity u_t in the inertial subrange of isotropic turbulence [14] is given by $u_t = \sqrt{2}\varepsilon^{1/3} d^{1/3}$.

NUMERICAL PROCEDURE

In the modelling of micro-bubble flows, two sets of governing equations for momentum were solved. The generic CFD code ANSYS CFX 11 [15] was employed as a platform for two-fluid flow computation. The built-in Inhomogeneous and MUSIG models were adopted for our numerical simulations. Figure 1 shows the schematic diagram of the numerical model used in our computations. The numerical simulations were performed with a velocity inlet and a pressure outlet, on the left and right side of the 2D computational domain respectively. The top wall is modelled as a friction-free boundary condition, wherein the height of the computational domain reflects half the height of the original test section. The bottom part of the domain has been divided into three distinct sections, section 1 & 3 were modelled as walls emulating the experimental boundary conditions, where as the section 2 is modelled as the inlet boundary condition for our gas inlet imitating the experimental conditions of gas injection though the porous plate. A uniform liquid velocity was specified at the inlet of the test section, different gas flow rates were specified along the section 2 of the computational domain, the free stream velocities and the gas injection rates used in the simulations are summarized in Table 1. An area permeability of 0.3 which lies in line with the sintered metal used in the experiments and also employed in the numerical work of Kunz et al [16] is used all along section 2 for gas injection purposes. At the outlet, a relative averaged static pressure of zero was specified. For all flow conditions, reliable convergence were

achieved within 2500 iterations when the RMS (root mean square) pressure residual dropped below 1.0×10^{-7}. A fixed physical time scale of 0.002s is adopted for all steady state simulations.

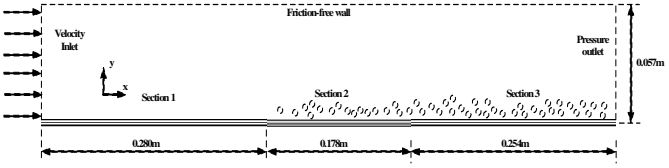

Figure 1 Schematic diagram of the numerical model

In handling turbulent micro-bubble flow, unlike single phase fluid flow problem, no standard turbulence model has been customized for two-phase (liquid-air) flow. Nevertheless, numerical investigation revealed that standard k-ε model predicted an unrealistically high gas void fraction peak close to wall [17, 18]. The k-ω based Shear Stress Transport (SST) model by Menter [19] provided more realistic prediction of void fraction close to wall. The SST model is a hybrid version of the k-ε and k-ω models with a specific blending function. Instead of using empirical wall function to bridge the wall and the far-away turbulent flow, the k-ω model solves the two turbulence scalars right up to the wall boundary. This approach eliminates errors arising from empirical wall function and thus provides better prediction at the near wall region. The SST model is thereby employed in the present study. Moreover, to account for the effect of bubbles on liquid turbulence, the Sato's bubble-induced turbulent viscosity model [20] has been adopted as well. The MUSIG model used through out the simulation had been specified 10 groups of bubbles, diameters ranging from 100µm-1000µm.

Case	Air flow rate Q_a (m^3/s)	Water free stream velocity (m/s)	Re_L based on the total plate length
Q0-V14.2(C_{fo})	0	14.2	1.13 x 10^7
Q1-V14.2	0.001	14.2	1.13 x 10^7
Q2-V14.2	0.0015	14.2	1.13 x 10^7
Q3-V14.2	0.002	14.2	1.13 x 10^7
Q4-V14.2	0.0025	14.2	1.13 x 10^7
Q5-V14.2	0.003	14.2	1.13 x 10^7

Table 1. Input boundary conditions for the computational model

RESULTS AND DISCUSSION

Air is injected through the 'section 2' of the computational domain, there by creating a micro-bubble flow. The depth of the domain was assumed to be 0.102m, in order to calculate the gas inlet volumetric flow rates though the section. The gas injection rates (Q_a) have been varied through the section and their skin friction co-efficients have been tabulated across. Figure 2 shows the comparison of our simulated skin friction ratios using both the numerical approaches against the experimental findings of Madavan et al [1] along varying gas injection rates (Q1-Q5). Herein, C_f & C_{fo} are the skin-friction co-efficients with and without the gas injection respectively. The skin-friction co-efficient throughout our numerical study have been obtained by averaging out the entire flat plate of 'section 3'. It can be seen that while MUSIG model seem to under predict for low gas flow rates (Q1-Q3), but they perform better at high flow rates (Q4 & Q5), wherein multiple sized bubbles can be found with high probability Whereas the Inhomogeneous model seem to over predict slightly at higher gas flow rates while emulating good values for low gas injection rates.

With the skin friction co-efficients showing fairly good comparison for the two-fluid inhomogeneous model, it can be further investigated to study the various mechanisms of drag reduction. To begin with the mean streamwise velocities of the carrier phase are scrutinized. Figure 3 shows the plot of mean streamwise liquid velocity along varying gas injection rates, a clearly marked change in the velocity profile can be seen with a subsequent increase in the gas flow injection rates, which is quite in relation to the large amount of micro-bubbles present along the boundary layer.

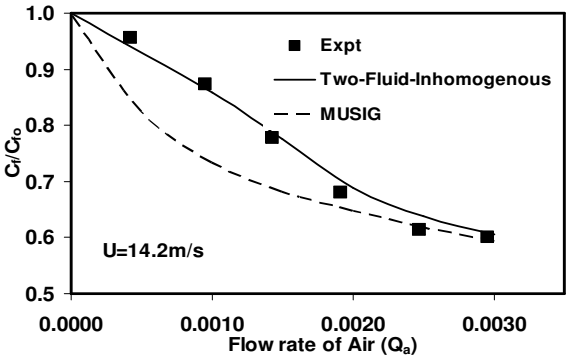

Figure 2 Comparison of computed plate drag co-efficient Inhomogeneous & MUSIG models

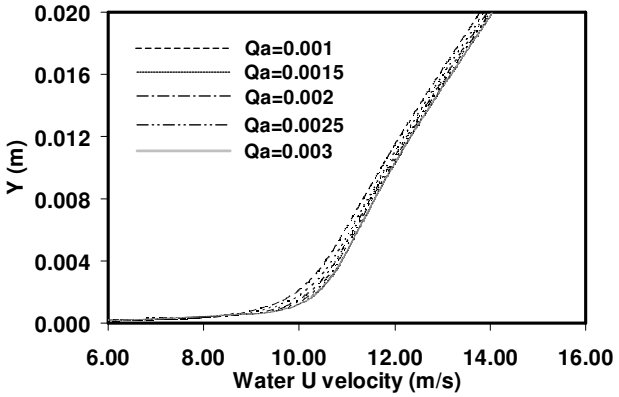

Figure 3 Velocity profiles for varying gas injection rates

The streamwise velocities, reveal that with the increase in the gas flow rates, there is a subsequent and a gradual increase in the streamwise velocities, however, a close look at figure 4 shows the exact opposite, in this figure, the velocity profiles of the liquid phase for the micro-bubbles laden flows have been normalized with the corresponding single phase liquid velocities along the length of the boundary layer, where by any velocity change felt in the carrier liquid phase is reflected as an exit of the ratio from unity, from the figure it can be revealed, that there is a marked decrease in the mean streamwise velocities with a subsequent increase of the gas injection rates, it is also seen, that the flow undergoes a maximum change in the mean velocity of about 40% for the highest gas flow rate, while it is quite nominal and about 13% for the lowest gas injection rate, this trend keeps increasing until a y^+ value of 100, aftermath of which there is a spike for the largest of the three gas flow rates and then a downward trend follows.

These findings reported above are in lines with the DNS findings [3], wherein the presence of micro-bubbles in the turbulent boundary layer results in a local positive divergence of the fluid velocity, $\nabla \bullet U > 0$, creating a positive mean velocity normal to (and away from) the wall which in turn, reduces the mean streamwise velocity and displaces the quasi-streamwise longitudinal

vortical structures away from the wall. The shifting of the vortical structures away from the wall indicates that the 'sweep' and 'ejection' events [21], which are located respectively at the downward and upward sides of these longitudinal vortical structures, are moved farther away from the wall, thereby reducing the intensity of wall streaks along the wall and consequently reducing the skin-friction. It was also reported that there is shift with respect to the location of peak Reynolds stress production away from the wall, thus reducing the production rate of turbulence kinetic energy and enstrophy.

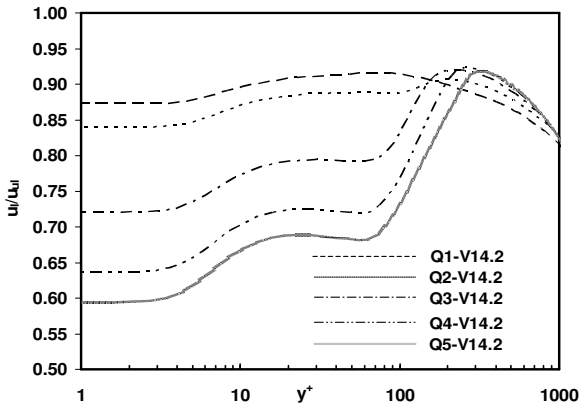

Figure 4 Change in the mean flow velocity for the carrier phase along the boundary layer

Figure 5 shows the plot of water normal velocity through varying gas injection rates, it can be seen that there is generally an increasing trend in the velocities and then a decrease which is followed by a maximum peak, and this is in direct relation to the loss incurred by the flow along the streamwise direction, across varying gas injection rates. There is also a sudden spike in the normal velocities within a y^+ range of 60-120. However, the onset of the increase and the occurrence of the maximum differ in accordance to the gas injection rates. For the three higher injection rates (Q3-Q5) the location of the start of sudden increase and the occurrence of maximum seems to occur more or less in unison, but their magnitude of maximum normal velocities differ wide apart. While for the lower gas injection rates (Q1 & Q2) the location and the magnitude are more distinct and separated wide apart. It can also be seen that the unladen wall normal velocity is quite smaller in lieu with the laden normal velocities. This can be further confirmed from the contour plot of the air void fraction along the boundary layer as shown in figure 6, for the highest air flow rate considered in our study, where there is a small layer of water, which is immediately followed on the top by a thick layer of air and then followed again by water, herein due to the inherent presence of the micro-bubbles in the middle section caused an upward shift in the water normal velocities.

Figure 7 shows the plot of non-dimensional streamwise velocities along the boundary layer for varying gas flow rates at the outlet. The presence of the micro bubbles can be strongly felt for a $y^+ \geq 10$, where in there is a gradual thickening of the buffer layer, with an upward shift of the logarithmic region, while the inner layer seems more or less unaltered. With these findings, it can be ascertained that the important aspect in achieving drag reductions is the accumulation of the micro bubbles within a critical zone in the buffer layer, how small they may be, they have a pronounced effect in the drag reduction. This is in lieu with the experimental findings [4], whereby high drag reductions were reported due the accumulation of the micro bubbles within a range of $15 \geq y^+ \leq 30$, they also acknowledge from their studies that a high percentage drag reductions can be achieved with low void fractions. The readers are advised that the Reynolds number of the carrier phase water is many times greater than that of the experimental case compared above.

The plot depicted in the figure 8 demonstrates the turbulent modification (TM) of the liquid phase in the presence of the micro-bubbles and is given by the ratio of the micro-bubble laden flow r.m.s streamwise velocity to the unladen r.m.s streamwise velocity. These plots signify that any TM felt in the carrier liquid phase is reflected as an exit of the ratio from unity. It can be seen from the plot, across various gas injection rates a marked attenuation is felt up to a distance along the boundary layer and then a subsequent increase, which is attributed towards the turbulence enhancement of the liquid phase. It is also worthwhile to note that the flow has a tendency to attenuate more for higher gas flow rates. On the other hand there is a turbulence augmentation effect pronounced more in the outer layer of the boundary. The marked attenuation felt for a small distance from the wall is attributed to the presence of a thin lining of liquid all along the wall (as explained above). However, in order to explain the augmentation of the turbulence felt within the boundary, the "bubble-repelling" and the "bubble-rising" events observed from the experiments of Murai et al [22] is used From their findings, it is outlined that the vertical rise velocity of the bubble or the "bubble-rising" event towards the wall is only about 5% of the streamwise velocity, after which the bubble reaches equilibrium with its surroundings and starts its journey back through the "bubble-repelling" event away from the wall, but however this downward journey accounts for 25% of the streamwise velocity.

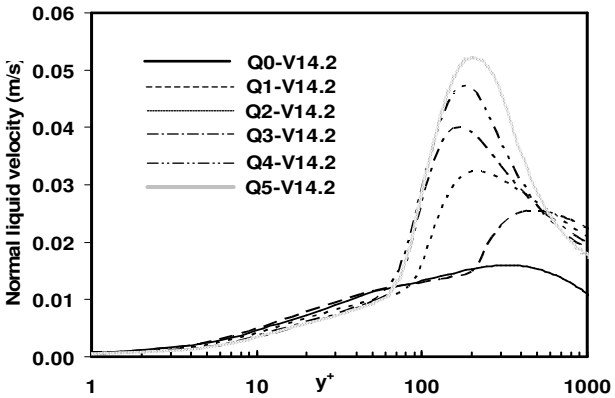

Figure 5 Liquid normal velocities for the carrier phase along the boundary layer

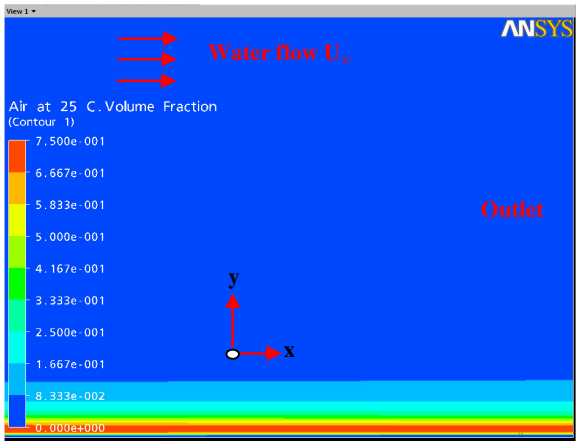

Figure 6 Air void fraction contour plot for Q5-V14.2

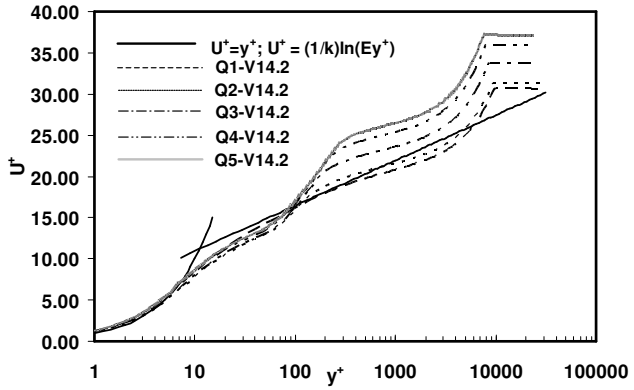

Figure 7 Change in the boundary layer for varying flow rates

Although the aforementioned experimental observations refer to individual bubble motion which can only be tracked numerically using Lagrangian approach, the phenomenon of turbulence augmentation in the carrier phase is taken care in our simulation through the SATO [19] model, which accounts for the additional viscosity generated through the bubble slip velocity, wherein the vortices are formed behind the bubbles by their motion, thereby causing an increase in the turbulence levels in the outer layer of the boundary. It can also be seen that this turbulence enhancement is more pronounced in the outer layer of the boundary, while most part of the inner and the buffer layer experiences attenuation.

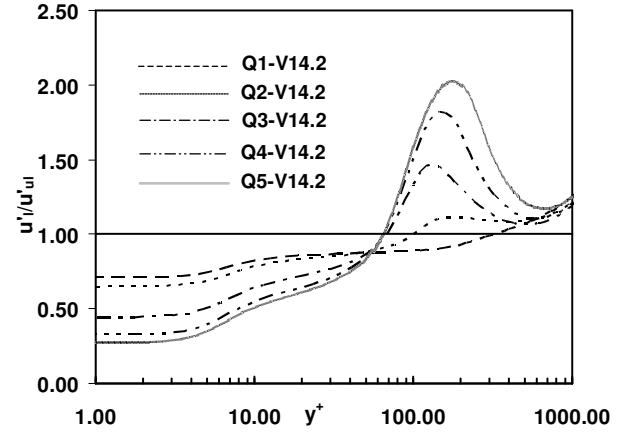

Figure 8 Turbulence Modulation (TM) along the boundary layer

CONCLUSION

Turbulent micro-bubble laden flow has been investigated with the help of two numerical models namely the two-fluid Inhomogeneous and MUSIG models. Inhomogeneous model, which uses a fixed bubble diameter, shows a very good comparison of the skin-friction co-efficients with the experiment [1]. This model is further probed to study the various physical phenomenon's causing the drag reduction along the boundary layer, firstly it was observed that there is drop in the mean streamwise water velocities with a subsequent increase in the normal along varying gas injection rates. Secondly, the presence of the micro-bubbles caused turbulence attenuation for some distance along the boundary layer and later an augmentation was felt due to the shedding of the vortices behind the bubbles.

However, with respect to the drag reduction caused due to the presence of micro-bubbles in the turbulent boundary layer MUSIG model, which encompasses a distribution of the different bubble diameters, seem to show good predictions for higher gas flow rates while under predicting for lower gas flow rates. Further study is directed towards investigating the same, so as to purview a better understating of drag reduction using micro-bubbles.

ACKNOWLEDGEMENT

This work was partially supported by the DSTO and the first author was supported by IPRS research scholarship.

REFERENCES

[1] Madavan, N.K., Deutsch,S., Merkle,C.L., 1984. Reduction of turbulent skin friction by microbubbles. Physics of Fluids 27, 356-363.

[2] Skudarnov P.V., Lin C.X., 2006. Drag reduction by gas injection into turbulent boundary layer: Density ratio effect. International Jounral of Heat and Fluid Flow 27, 436-444.

[3] Ferrante, A., and Elghobashi, S., 2004. On the Physical Mechanisms of Drag Reduction in a Spatially Developing Turbulent Boundary Layer Laden with Microbubbles. Journal of Fluid Mechanics 503, 345–355.

[4] Villafuerte, J.O., Hassan, Y.A., 2006. Investigation of microbubble boundary layer using particle tracking velocimetry. Journal of Fluids Engineering 129, 66-79.

[5] Kitagawa, A., Hishida, K., Kodama, Y., 2005. Flow structure of micro-bubble laden turbulent channel flow measured by PIV combined with the shadow image technique. Experiments in Fluids 38, 466–475.

[6] Murai, Y., Fukuda, H., Oishi, Y., Kodama, Y., Yamamoto, F., 2007. Skin Friction Reduction by Large Air Bubbles in a Horizontal Channel Flow. International Journal of Multiphase Flow 33, 147-163.

[7] Ishii, M. 1975. Thermo-fluid dynamic theory of two-phase flow. Eyrolles, Paris.

[8] Drew, D.A., Lahey Jr., R.T., 1979. Application of general constitutive principles to the derivation of multidimensional two-phase flow equation. Int. J. Multiphase Flow, 5, 243-264.

[9] Ishii, M., Zuber, N., 1979. Drag coefficient and relative velocity in bubbly, droplet or particulate flows. A.I.Ch.E. Journal, 5, 843-855.

[10] Kumar, S., Ramkrishna, D., 1996a. On the solution of population balance equations by discretisation – I. A fixed pivot technique. Chem. Eng. Sci., 51, 1311-1332.

[11] Luo, H., Svendsen, H., 1996. Theoretical model for drop and bubble break-up in turbulent dispersions. A.I.Ch.E Journal, 42, 1225-1233.

[12] Prince, M.J., Blanch, H.W., 1990. Bubble coalescence and break-up in air sparged bubble columns. A.I.Ch.E Journal, 36, 1485-1499.

[13] Chesters, A.K., Hoffman, G., 1982. Bubble coalescence in pure liquids, Appl. Sci. Res., 38, 353-361.

[14] Rotta, J.C. (1972). Turbulente Stromungen, Teubner B.G., Stuttgart,1972.

[15] ANSYS, (2006). CFX-11 User Manual. ANSYS CFX.

[16] Kunz, R. F., Deutsch, S., and Lindau, J. W., 2003. Two Fluid Modelling Of Microbubble Turbulent Drag Reduction. ASME Paper No. FED2003-45640, Proceedings of FEDSM'03: 4TH ASME-JSME Joint Fluids Engineering Conference,Honolulu, Hawaii, July 6–11, ASME, New York.

[17] Frank, T., Shi, J., Burns, A.D., 2004. Validation of Eulerian multiphase flow models for nuclear safety application, in: Proceeding of the Third International Symposium on Two-Phase Modelling and Experimentation, Pisa, Italy

[18] Cheung, S.C.P., Yeoh, G.H., Tu, J.Y., 2006. On the modelling of population balance in isothermal vertical bubbly flows – average bubble number density approach. Chem. Eng. Process., in Press
[19] Menter, F.R. 1994. Two-equation eddy viscosity turbulence models for engineering applications. AIAA J., 32, 1598-1605.
[20] Sato, Y., Sadatomi, M., Sekoguchi, K., 1981. Momentum and heat transfer in two-phase bubbly flow – I. International Journal of Multiphase Flow 7, 167-178.
[21] Robinson, S.K., 1991. Coherent motions in the turbulent boundary layer. Annual Review of Fluid Mechanics 23, 601-639.
[22] Murai, Y., Oishi, Y., Takeda, Y., Yamamoto, F., 2006. Turbulent shear stress profiles in a bubbly channel flow assessed by particle tracking velocimetry. Experiments in Fluids 41, 343–352.